



The thermal diode and insulating potentials of a vertical stack of parallelogrammic air-filled enclosures

Thierry Villeneuve, Matthieu Boudreau, Guy Dumas*

CFD Laboratory LMFN, Département de Génie Mécanique, Université Laval,
Québec, Canada, G1V 0A6

Postprint, 2017 - International Journal of Heat and Mass Transfer

Published version available online at: <https://doi.org/10.1016/j.ijheatmasstransfer.2016.12.067>

Abstract

This paper focuses on the interaction and the contribution of the three modes of heat transfer in a stack of parallelogrammic air-filled cavities separated by solid partition walls. The thermal diode potential and the high insulating character of such structures are the main interests of this investigation. The inclination angle, the emissivity of the inner boundaries of the cavity as well as the thickness and the thermal conductivity of the partition walls are the parameters varied in this study. Their respective contributions to the total Nusselt number are assessed. The two-dimensional fluid cavities studied in this work are characterized by an aspect ratio of 1. The vertical boundaries of the enclosures are considered isothermal at specified hot and cold temperatures, and the inclination angle of the partition walls is varied from -60° to 60° with respect to the horizontal. Numerical simulations are carried out using a finite-volume solver. It is shown that the total Nusselt number is highly sensitive to the emissivity of the inner boundaries of the cavities and thus, to the heat transfer through radiation. Moreover, it is found that the conduction heat transfer in the partition walls also plays an important role in most of the cases investigated. The importance of these two modes of heat transfer results in a significant decrease in both the thermal diode potential and the insulating character of the enclosures compared to the classic case for which only convection heat transfer is considered. Nonetheless, this study suggests that a vertical structure composed of a stack of parallelogrammic air-filled enclosures could be successfully designed to provide a practical and economically interesting alternative to polystyrene panels.

Keywords: Natural convection, Three-mode heat transfer, Parallelogrammic cavity, Thermal diode, Radiation, Conduction

1. Introduction

Over the past decades, several investigations have been directed towards the development of approximate solution methods for applications involving natural convection. The particular case of free convection in cavities, which is quite prevalent in practice, has mainly retained the attention. Many authors have performed theoretical studies on natural convection heat transfer across cavities [1, 2, 3]. Early on in the numerical simulation era, the differentially heated square cavity became a classic numerical problem.

Indeed, natural convection in closed cavities has been investigated in numerous occasions and many different geometries have been studied over the years. For example, many authors have oriented their research towards cylindrical shapes [4, 5], while others worked on triangular cavities [6, 7]. Nevertheless, the most widely studied geometry in the literature remains the 2D square, rectangular or parallelogrammic cavity.

For these types of cavity, the effects of many parameters, such as the Rayleigh number (Ra), the Prandtl number (Pr) and the aspect ratio (h/L), have already been extensively studied [1, 8, 9, 10, 11]. Generally, a higher Rayleigh number results in an increased heat transfer across the cavity and can eventually

lead to unsteady phenomena and turbulence, while moderate variations of the Prandtl number does not significantly influence the general behavior of the flow in the cavity [12, 13, 14].

From a more practical point of view, several papers have dealt with the impact of the inclination angle (ϕ) of the partition walls bounding the upper and lower parts of the parallelogrammic cavity [10, 15, 16, 17, 18]. It has been shown that the convection heat transfer is highly affected by the inclination angle of the partition walls. As shown in Figure 1, the convective motion of the fluid is much more important when the vertical hot boundary is located *below* the vertical cold boundary (positive ϕ), while a vertical hot boundary *above* the cold one (negative ϕ) can even lead to a complete stratification in the cavity and, ultimately, to essentially pure conduction heat transfer in a stagnant fluid. Therefore, the heat transfer through a given inclined cavity has two different values depending on the side of the hot boundary. This attractive behavior has been confirmed by many authors who refer to the parallelogrammic cavity as a thermal diode cavity [15, 18, 19]. Indeed, several numerical and experimental studies have shown that the convection Nusselt number is strongly reduced when the inclination angle (ϕ) is negative [10, 11, 17].

In addition to the applications that could benefit from the thermal diode behavior of such cavities, it could also be interesting in practice as an insulating wall. The idea of using

*Corresponding author - gumas@gmc.ulaval.ca

Nomenclature

Variables

e_g	unit gravity vector = (0, -1)
F_{ij}	view factor matrix
g	gravitational acceleration [ms^{-2}]
h	height of the hot and the cold boundaries of the cavity [m]
J	radiosity [Wm^{-2}]
k_f	thermal conductivity of the fluid [$\text{Wm}^{-1}\text{K}^{-1}$]
k_s	thermal conductivity of the solid partition walls [$\text{Wm}^{-1}\text{K}^{-1}$]
L	distance between the hot and the cold boundaries [m]
p	pressure [Pa]
n	local unit vector normal to a boundary and directed towards the considered region
\bar{q}'_{cond}	mean conduction heat transfer rate per unit depth in the partition walls, Equation (10) [Wm^{-1}]
\bar{q}'_{conv}	mean convection heat transfer rate per unit depth in the fluid cavity, Equation (8) [Wm^{-1}]
\bar{q}'_{rad}	mean radiation heat transfer rate per unit depth in the fluid cavity, Equation (9) [Wm^{-1}]
q'_{ref}	reference conduction heat transfer rate per unit depth in the enclosure, Equation (7) [Wm^{-1}]
q''_r	radiative thermal heat flux, Equation (4) [Wm^{-2}]
t	thickness of the solid partition walls [m]
T	temperature [K]
T_0	mean temperature = $(T_H + T_C)/2$ [K]
T_C	temperature of the cold boundary [K]
T_H	temperature of the hot boundary [K]

u	velocity vector = (u, v) [ms^{-1}]
x	position vector = (x, y) [m]
α	thermal diffusivity of the fluid [m^2s^{-1}]
β	coefficient of volumetric expansion of the fluid [K^{-1}]
θ	temperature difference scale = $T_H - T_C$ [K]
ν	kinematic viscosity [m^2s^{-1}]
ρ	density [kgm^{-3}]
σ	Stefan-Boltzmann constant [$\text{Wm}^{-2}\text{K}^{-4}$]
ψ	stream function [m^2s^{-1}]

Dimensionless physical parameters

h/L	aspect ratio of the cavity
k_s/k_f	thermal conductivity ratio
Pr	Prandtl number = ν/α
Ra	Rayleigh number = $g\beta\theta L^3/\alpha\nu$
t/L	thickness ratio of the solid partition walls
T_0^*	normalized mean temperature = T_0/θ
ϵ	emissivity
$\frac{\sigma T_0^4}{k_f\theta/L}$	relative radiation level
ϕ	inclination angle of the solid partition walls with respect to the horizontal

Dimensionless coefficients

Nu	Nusselt number
ξ_{60}	thermal diode coefficient

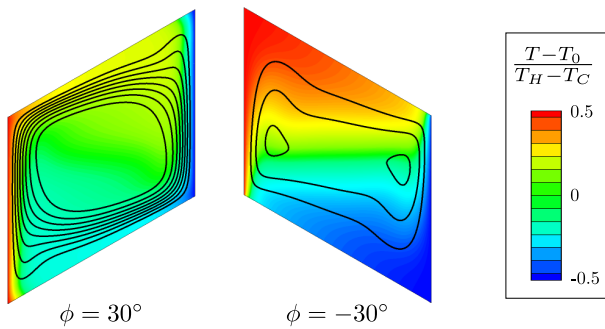


Figure 1: Temperature fields (colored background) and stream functions (black lines, $\Delta\psi^* = 0.0041$) for air-filled cavities with adiabatic upper and lower boundaries and isothermal vertical boundaries (the hot boundary is located on the left).

a stack of piled-up air-filled cavities instead of a full panel of insulating material is very attractive. Indeed, a wall composed of air-filled cavities that would have the same thermal properties as an insulating material would have major economic and environmental advantages due to the reduction of the amount of material needed. To investigate this possibility, the three modes of heat transfer must be considered in a structure composed of multiple piled-up cavities.

Most of the studies in the field have investigated the case of a single cavity with adiabatic upper and lower boundaries. Only a few authors have considered more than one fluid cavities [11, 18, 20, 21], either fully or partially separated by conductive solid partition walls, even if one expects to use walls composed of several such cavities. Moreover, most of the studies that have been performed on the thermal diode cavity have not considered radiation even if it has been shown that this heat transfer mode

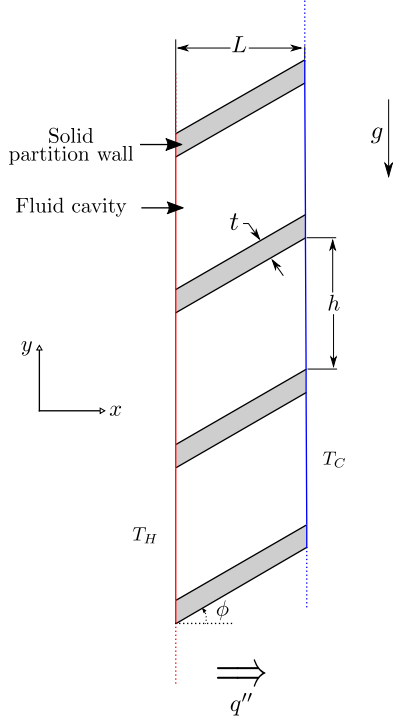


Figure 2: Sketch of the infinite stack of parallelogrammic air-filled cavities separated by conductive solid partition walls.

can become quite significant [21, 22, 23]. To the authors' best knowledge, the study of multiple cavities involving the three modes of heat transfer has not yet been investigated in the literature despite its relevance in many applications.

The objective of the present study is to assess the individual contribution of each of the three heat transfer modes, as well as how they interact with each other in an infinite stack of parallelogrammic cavities separated by conductive solid partition walls, as shown in Figure 2. This general problem is governed by nine dimensionless parameters (see nomenclature), which makes it a formidable challenge. In this initial phase of our investigation, we have fixed five of these nine parameters to focus on the general trends first. Thus, we have varied the inclination angle (ϕ), the thickness and the thermal conductivity ratios of the solid partition walls (t/L and k_s/k_f) and the emissivity of the inner boundaries of the cavities (ϵ) in order to show their effect on the thermal diode potential and on the total heat transfer.

In order to analyze the importance and the contribution of the three heat transfer modes separately, we proceed in three steps. First, a single cavity with adiabatic upper and lower boundaries is presented (Figure 3a). The pure-convection heat transfer is briefly discussed using a cavity without partition walls and without considering radiation. This simple case, which has been studied thoroughly in the literature, is used as a reference to evaluate the impact of the other heat transfer modes. In a second step, the effects of considering conductive partition walls and radiating inner boundaries are then investigated separately before combining the three modes in a single enclosure (Figure 3b). It is shown that the thermal diode potential is drastically reduced when conduction and radiation are taken into account.

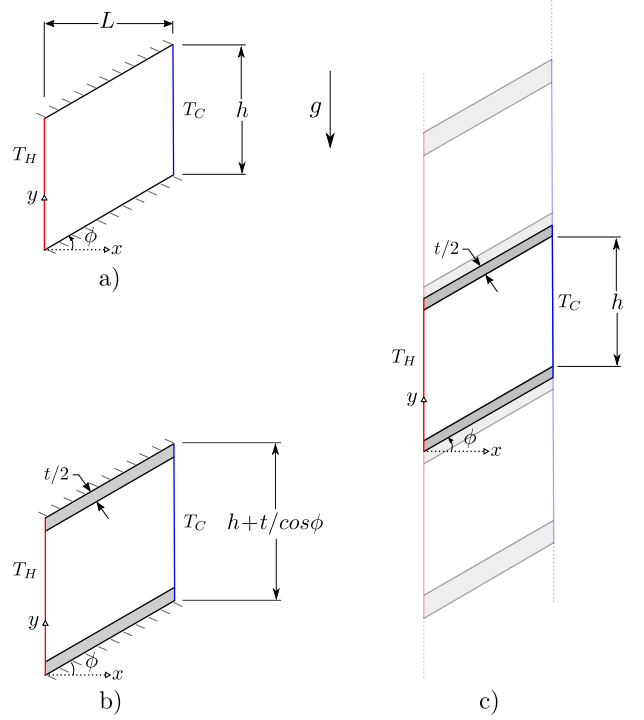


Figure 3: Schematic representation of the three physical domains investigated: a) Single adiabatic cavity, b) Single adiabatic enclosure with solid partition walls, c) Infinite structure of piled-up enclosures (with periodicity conditions applied at the junction between light gray and dark gray regions).

In the third step, the thermal diode potential and the insulating performances of an infinite structure of piled-up enclosures is presented.

2. Physical case

As stated previously, this investigation aims at quantifying the relative contribution of each of the three modes of heat transfer and their interaction in an infinite stack of enclosures composed of air-filled cavities and solid partition walls. In a more practical point of view, this work also aims at determining the thermal diode and insulating potentials of such a structure. Three different physical domains are considered in order to be able to discriminate the individual contribution of each heat transfer mode. As shown in Figure 3, the first domain (a) consists of a single air-filled cavity with adiabatic upper and lower boundaries. The second one (b) is also a single adiabatic cavity, but solid partition walls are added to the geometry in order to consider the conduction heat transfer taking place in these solid regions. The third physical domain (c) is an infinite stack of enclosures composed of a series of air-filled cavities and solid partition walls. This infinite structure can be represented by a single enclosure (including two half partition walls) using periodicity conditions imposed at the junction between light gray and dark gray regions in the partition walls of Figure 3c. It thus corresponds to the domain of Figure 3b with periodic boundary conditions instead of adiabatic boundary conditions. Note that the term “cavity” is used to describe the fluid region

of the enclosure (without considering the solid regions) while the term “enclosure” refers to the fluid cavity along with the solid partition walls.

In these two-dimensional geometries, the height of the air-filled cavities (h) and the distance between the hot and the cold vertical boundaries (L) remain equal to each other, leading to a fixed aspect ratio $h/L = 1$. A Rayleigh number of $Ra = 5 \times 10^5$ is considered (which represents a temperature difference of $\theta = 28.5$ K across a $L = 5$ cm cavity filled with air) together with a Prandtl number of $Pr = 0.71$. Two of the dimensionless parameters governing radiation are fixed, namely the relative radiation level $\sigma T_0^4 / (k_f \theta / L) = 24.65$ and the normalized mean temperature $T_0^* = 9.75$. These two parameters are defined in section 2.1. The energy transfer occurs between the vertical boundaries which are maintained respectively at a hot (T_H) and a cold (T_C) specified temperature. The upper and lower boundaries of the enclosures can be inclined by an angle between -60° to 60° with respect to the x -axis.

Two values of dimensionless thicknesses of the partition walls ($t/L = 0.01$ and 0.1) and two values of thermal conductivity ratios ($k_s/k_f = 1$ and 10) are tested. Regarding the radiation heat transfer, three different emissivity values ($\epsilon = 0, 0.1$ and 0.9) are considered. Lastly, the heat transfer calculations are carried out for five different inclination angles ($\phi = -60^\circ, -30^\circ, 0^\circ, 30^\circ$ and 60°).

2.1. Mathematical formulation

2.1.1. Governing equations

Considering deep (in the z -direction) parallelogrammic cavities, the physics pertaining to such cavity is assumed two-dimensional. Fusegi & al. [24] compared the results of a three-dimensional cavity with a two-dimensional one. They showed that even if there is a transverse z -component velocity in the 3D cavity, it is one order of magnitude smaller than the components in the other directions and it does not significantly affect the total heat transfer at the Rayleigh number considered in this study. Moreover, to validate the present 2D assumption, we have carried out simulations in three-dimensional enclosures with a depth five times larger than their length ($5L$) for many of the parametric cases in this study. We have found that the end effects occurring in the cavity are typically confined within a distance L from the ends and that they affect only marginally the physical fields (velocity and temperature) and the total heat transfer in the enclosure.

Furthermore, it has been shown that for a Rayleigh number smaller than 1.3×10^7 (with $Pr = 0.71$ and $h/L = 1$), such as in this study, the flow in the cavities is laminar and steady [10]. As a matter of validation, three-dimensional unsteady simulations in parallelepipedic enclosures have been computed. Our results showed that the flow is indeed steady, thereby allowing us to carry out steady state numerical simulations.

For natural convection of air in cavities of that kind and under a temperature difference smaller than 30 K, the validity of the Boussinesq approximation that is used here has already been verified [11, 18]. Air inside the enclosures is therefore considered incompressible with constant physical properties, except

for the density variations in the buoyancy term. The governing equations in the fluid region are thus the continuity (1), the Navier-Stokes (2) and the energy (3) equations [25]:

$$\nabla^* \cdot \mathbf{u}^* = 0, \quad (1)$$

$$\mathbf{u}^* \cdot \nabla^* \mathbf{u}^* = -\nabla^* p^* + \left(\frac{Pr}{Ra}\right)^{1/2} \nabla^{*2} \mathbf{u}^* + (T^* - T_0^*) \mathbf{e}_g, \quad (2)$$

$$\mathbf{u}^* \cdot \nabla^* T^* = \frac{1}{(Ra Pr)^{1/2}} \nabla^{*2} T^*, \quad (3)$$

where all the star variables and operators above are dimensionless, being normalized by their appropriate reference quantity: reference length L , temperature scale $\theta = T_H - T_C$, reference velocity $\sqrt{\beta \theta g L}$ and pressure scale $\rho \beta \theta g L$.

In Equation 2, T_0^* is the normalized mean temperature defined as $(T_H + T_C)/2\theta$. Regarding the conduction in the solid partition walls, it is governed by Equation 3 where the velocity (\mathbf{u}^*) is equal to zero. In both the fluid and the solid regions, the thermal properties are assumed to be uniform and constant.

2.1.2. Boundary conditions

The velocity (\mathbf{u}^*) is set to zero on each boundary of the cavity (no-slip condition). Moreover, for all the parametric cases investigated, the dimensionless temperature of the vertical hot boundary (T_H^*), located on the left side of the enclosure, is equal to 10.25 ($T_H^* - T_0^* = 0.5$), while the dimensionless temperature of the vertical cold boundary (T_C^*) located on the right side is 9.25 ($T_C^* - T_0^* = -0.5$). The thermal conditions for the other boundaries of the enclosure depend on the physical domain that is considered. For the domain shown in Figure 3a and 3b, the uppermost and lowermost boundaries of the enclosure are considered adiabatic. For the domain shown in Figure 3c, periodicity conditions are applied to the upper and the lower boundaries of the enclosure for both the temperature and the temperature gradient. For cases involving radiation, air is considered as a non-participating medium, so that the radiation heat transfer only occurs on the inner boundaries of the cavities. Making the assumptions that these boundaries are opaque, gray and diffusive, the dimensionless radiation heat transfer is therefore given by:

$$q_r''^* = \frac{\epsilon}{1 - \epsilon} \left(\left(\frac{T^*}{T_0^*} \right)^4 - J^* \right), \quad (4)$$

where ϵ is the emissivity and J^* is the dimensionless radiosity. Both $q_r''^*$ and J have been normalized using a reference radiative heat flux σT_0^4 .

The radiosity is computed using the following relation for the i^{th} panel along each inner boundary of the cavity:

$$\frac{\epsilon_i}{1 - \epsilon_i} J_i^* + \sum_{j=1}^N F_{ij} (J_i^* - J_j^*) = \frac{\epsilon_i}{1 - \epsilon_i} \left(\frac{T_i^*}{T_0^*} \right)^4, \quad (5)$$

where N is the total number of panels on the inner boundary coinciding with the fluid finite volume edges along that boundary and F_{ij} is the view factor matrix representing the portion of the radiating energy leaving boundary i that is intercepted by boundary j . In the numerical simulations, a radiosity value has been computed for each element of the fluid mesh that is in contact with an inner boundary of the cavity. In the present study, the normalized mean temperature (T_0^*) is set to 9.75, corresponding, for example, to a mean temperature (T_0) of 278 K and a temperature difference (θ) of 28.5 K.

At the junction between the fluid and the solid regions, the energy must be conserved, meaning that the following equation is satisfied:

$$\left(\frac{\partial T^*}{\partial \mathbf{n}^*}\right)_{fluid} + \frac{\sigma T_0^4}{k_f \theta / L} q_r'^* = -\frac{k_s}{k_f} \left(\frac{\partial T^*}{\partial \mathbf{n}^*}\right)_{solid}, \quad (6)$$

where \mathbf{n}^* is the normalized local unit vector normal to the boundary that is directed towards the considered region. Equation (6) introduces two of the nine dimensionless parameters, namely the parameter $\sigma T_0^4 / (k_f \theta / L)$ and the parameter k_s / k_f . For all the simulated cases in this study, the parameter $\sigma T_0^4 / (k_f \theta / L) = 24.65$.

2.2. Mathematical analysis

In order to compare the three heat transfer modes' contributions occurring either through the hot or the cold boundary of the enclosures, it is useful to define a dimensionless coefficient quantifying each of them. For convection heat transfer, the commonly used Nusselt number is given by the ratio between the convection heat transfer rate through the enclosure per unit depth and a reference heat transfer rate corresponding to conduction heat transfer in a stagnant fluid. This reference heat transfer rate is given by:

$$q'_{ref} = (h + t / \cos \phi) \frac{k_f \theta}{L}. \quad (7)$$

For the geometry used in this study, it is important to recall that the three modes of heat transfer do not occur on the same boundaries in the enclosures. The terms ‘‘convection’’ and ‘‘radiation’’ are used here to refer to the heat passing through the vertical boundaries of the cavity (vertical blue and red lines in Figure 4) while the term ‘‘conduction’’ refers to the heat passing through the vertical boundaries of the partition walls (vertical green lines in Figure 4). Consequently, in order to perform direct comparison between the three modes of heat transfer, the relative surface area on which a given heat flux takes place has to be considered since the fraction occupied by the vertical boundaries of the cavity and the vertical boundaries of the partition walls are not the same. Thus, the convection, radiation and conduction heat transfer rates through the enclosure per unit depth are computed as follows:

$$\bar{q}'_{conv} = -k_f \int_{\frac{1}{2}t/\cos\phi}^{h+\frac{1}{2}t/\cos\phi} \frac{\partial T}{\partial x} dy, \quad (8)$$

$$\bar{q}'_{rad} = \frac{\epsilon}{1 - \epsilon} \int_{\frac{1}{2}t/\cos\phi}^{h+\frac{1}{2}t/\cos\phi} |\sigma T^4 - J| dy, \quad (9)$$

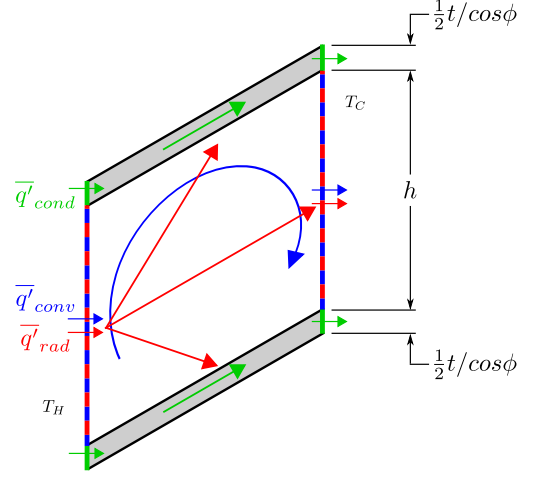


Figure 4: Schematic representation illustrating where the three modes of heat transfer take place in an enclosure. The vertical red and blue dash-lines represent the location of the convection and radiation heat transfer while the vertical green lines show the conduction heat transfer.

$$\bar{q}'_{cond} = -k_s \left[\int_0^{\frac{1}{2}t/\cos\phi} \frac{\partial T}{\partial x} dy + \int_{h+\frac{1}{2}t/\cos\phi}^{h+t/\cos\phi} \frac{\partial T}{\partial x} dy \right], \quad (10)$$

with the location of the coordinate system's origin as shown in Figure 3.

In this paper, we normalize the three heat transfer rates by the reference conduction heat transfer rate introduced in Equation (7). Therefore, the so-defined Nusselt numbers and the total Nusselt number are given by:

$$\bar{Nu}_{conv} \equiv \frac{\bar{q}'_{conv}}{q'_{ref}}, \quad (11)$$

$$\bar{Nu}_{rad} \equiv \frac{\bar{q}'_{rad}}{q'_{ref}}, \quad (12)$$

$$\bar{Nu}_{cond} \equiv \frac{\bar{q}'_{cond}}{q'_{ref}}, \quad (13)$$

$$\bar{Nu}_{tot} = \bar{Nu}_{conv} + \bar{Nu}_{rad} + \bar{Nu}_{cond}. \quad (14)$$

The integrals in Equations 11 to 13 can be computed either on the hot or the cold boundary ($x = 0$ or $x = L$). Although the total Nusselt number is necessarily the same on both boundaries, each of the three contributions differ slightly depending on which boundary the integrals are evaluated on when radiation is taken into account ($\epsilon \neq 0$). In this paper, we use the average of the values evaluated on both the hot and cold boundaries to report our Nusselt numbers \bar{Nu}_{conv} , \bar{Nu}_{rad} and \bar{Nu}_{cond} .

In order to compare the thermal diode potential between the simulated cases, we define a thermal diode coefficient (ξ_{60}):

$$\xi_{60} \equiv \frac{\bar{Nu}_{tot}|_{\phi=60^\circ}}{\bar{Nu}_{tot}|_{\phi=-60^\circ}}. \quad (15)$$

A large value of the thermal diode coefficient (ξ_{60}) thus corresponds to a case for which the total heat transfer at $\phi = 60^\circ$ is much larger than it is at $\phi = -60^\circ$. A similar definition can also be used for ξ_{30} (cases at $\phi = \pm 30^\circ$), but its value is found to be always smaller than ξ_{60} for the parametric cases considered in this study. We do not assume that ξ_{60} corresponds to the maximum thermal diode coefficient possible, but we can assume that it is representative for the purpose of addressing the basic impact of the heat transfer modes.

3. Numerics and validation

Using ANSYS® Fluent [26], the problem is solved with a finite-volume method using a coupled pressure-velocity algorithm [27]. For the radiation model, a surface-to-surface (S2S) method considering opaque, gray and diffusive surfaces is used [26]. The convergence criteria for all equations is set to 10^{-6} except for the energy residual which is set to 10^{-10} . Smaller convergence criteria by two orders of magnitude have been tested and no significant differences were observed. As mentioned previously, the Boussinesq approximation is used to conduct the simulations. In order to guarantee the validity of this approximation, some parametric cases have been computed considering variable physical properties for air, i.e., without using the Boussinesq approximation. The results obtained were essentially unchanged (less than 1% for the Nusselt numbers and the maximum stream function values), so we can confidently assume the Boussinesq approximation to be valid for the parametric cases treated in this study.

The mesh that has been used to carry out the simulations consists of quadrilateral elements which are parallel to the vertical boundaries and to the partition walls, as shown in Figure 5. The thickness of the first layer of elements next to the boundaries,

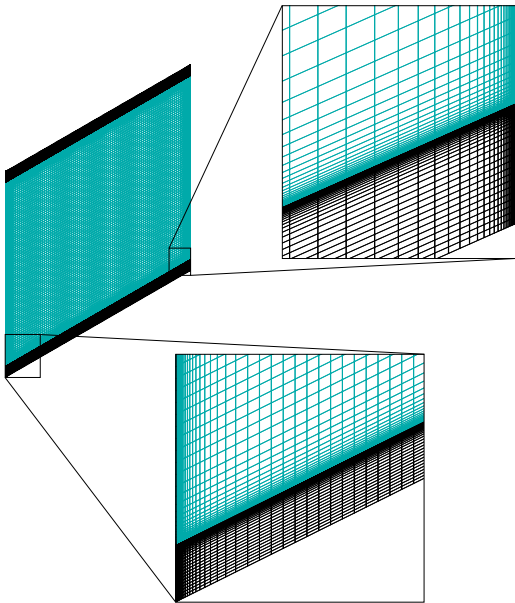


Figure 5: Mesh used for an enclosure with solid partition walls at an inclination angle of 30° ($t/L = 0.1$).

both in the fluid and in the solid regions, is $10^{-5}L$, which is much thinner than the thermal boundary layer providing a sufficiently fine discretization near those solid boundaries. We have verified that the same mesh resolution can be used for each parametric case. Consequently, the number of elements increases with the inclination angle. For the single cavity, the number of elements is 150×150 , 150×165 and 150×230 for inclination angles of 0° , 30° and 60° respectively. The entire thin partition wall ($t/L = 0.01$) is divided into 60 vertical elements while about 100 elements are used for the thicker partition wall ($t/L = 0.1$). The solutions obtained are all mesh-independent. Indeed, a finer and a coarser meshes have been tested and the solutions were essentially unchanged. Table 1 shows the grid sensitivity analysis for the case of an infinite structure of enclosures at an inclination angle of 60° . Based on these results, the resolution used for the mesh composed of 60 800 elements has been chosen to carry out the parametric study.

Table 1: Grid sensitivity analysis for an infinite structure of enclosures with solid partition walls and radiation ($t/L = 0.1$, $k_s/k_f = 10$ and $\epsilon = 0.9$) at an inclination angle of 60° .

Number of cells	ψ_{max}^*	\overline{Nu}_{tot}
28 600	0.0609	8.358
60 800	0.0607	8.361
160 000	0.0607	8.361

In order to further validate the main features of the numerical methodology used in this study, some comparisons with the benchmark solution presented by De Vahl Davis & Jones [3] have been performed for the pure-convection cavity differentially heated. For the combined convection-conduction heat transfer problem, the methodology used in the present work has been compared to the work of Costa & al. [20] who considered air-filled enclosures partially separated by solid regions. The combined convection-radiation heat transfer calculations have also been compared with the results presented by Balaji & Venkateshan [23] who investigated the interaction between surface radiation and free convection in square cavities. Table 2 summarizes some of the quantities that have been compared with the literature. As it can be seen, our numerical methodology is in good agreement with all of these independent studies, giving us great confidence in the results presented in the next section.

Table 2: Comparison with various results presented in the literature. a) Pure-convection cavity with $Pr = 0.71$, $h/L = 1$, $\phi = 0^\circ$. b) Combined convection-conduction heat transfer with $Ra = 10^7$, $Pr = 0.73$, $h/L = 5$, $\phi = 0^\circ$ and $t/L = 0.001$. c) Combined convection-radiation heat transfer with $Ra = 5 \times 10^4$, $Pr = 0.728$, $h/L = 1$, $\phi = 0^\circ$, $T_0^* = 6.25$ and $\sigma T_0^4 / (k_f \theta / L) = 1.1025$.

a) Pure-convection cavity			
		Present study	De Vahl Davis & Jones [3]
max vertical velocity	$Ra = 10^5$	0.0807	0.0812
	$Ra = 10^6$	0.2604	0.2597
\overline{Nu}_{tot}	$Ra = 10^5$	4.523	4.519
	$Ra = 10^6$	8.812	8.800
b) Combined convection-conduction heat transfer			
		Present study	Costa & al. [20]
\overline{Nu}_{tot}	$k_s/k_f = 1$	3.552	3.600
	$k_s/k_f = 10$	3.585	3.634
	$k_s/k_f = 100$	3.872	3.970
	$k_s/k_f = 1\ 000$	4.845	5.029
c) Combined convection-radiation heat transfer			
		Present study	Balaji & Venkateshan [23]
\overline{Nu}_{rad}	$\epsilon = 0.1$	0.0374	0.0366
	$\epsilon = 0.9$	0.4261	0.4264
\overline{Nu}_{conv}	$\epsilon = 0.1$	3.619	3.491
	$\epsilon = 0.9$	3.593	3.566

4. Results and discussion

In this initial phase of our investigation, let us recall that we have fixed five of the nine dimensionless parameters governing this problem: $h/L = 1$, $Ra = 5 \times 10^5$, $Pr = 0.71$, $\sigma T_0^4 / (k_f \theta / L) = 24.65$ and $T_0^* = 9.75$. These values are consistent with an air-filled enclosure of about 5 cm width, a temperature difference of 28.5 K and a mean temperature of 278 K. The four free parameters that are varied are the emissivity of the inner boundaries of the cavities (ϵ), the thickness ratio of the partition walls (t/L), their thermal conductivity ratio (k_s/k_f) and their inclination angle (ϕ).

4.1. Single adiabatic enclosure

4.1.1. Pure-convection cavity

The first case of interest is the single cavity with adiabatic upper and lower boundaries (without solid partition walls and without radiation), as shown in Figure 3a. In this configuration, the only mode of heat transfer involved is convection. The results presented in this section will be used as a reference in order to compare the contributions of the other modes of heat transfer.

Figure 6 shows the convection Nusselt number as a function of the inclination angle for this adiabatic cavity. Note that the lines drawn between computed data points only serve to link the points together and do not serve to interpolate between them. As it can be observed, the inclination angle strongly affects the convection Nusselt number in the cavity. The high asymmetry of the curve qualitatively demonstrates the thermal diode potential that is discussed in many other works [10, 11, 18, 28]. For this specific configuration, the value of the thermal diode

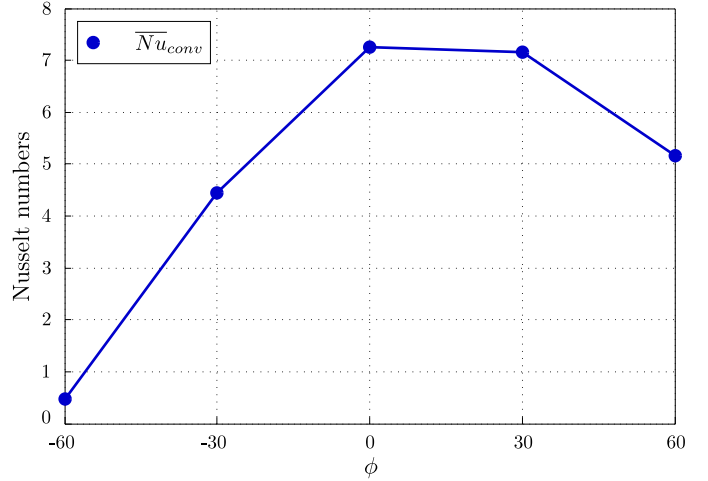


Figure 6: Convection Nusselt numbers as a function of the inclination angle for a single adiabatic cavity without partition walls and without radiation (physical domain of Figure 3a). Straight lines drawn between computed points are not intended for interpolation purposes.

coefficient is $\xi_{60} = 10.8$. It means that the total heat transfer across the cavity is 10.8 times smaller at an inclination angle of -60° in comparison with the one at an angle of 60° .

The results shown in Figure 6 are in agreement with the previous works mentioned above. Although it does not appear on the graph, it is interesting to note that the maximum heat transfer does not occur at 0° . Indeed, at an inclination angle of 15° , a Nusselt number of 7.47 is obtained. The same observation has also been made by Baïri & al. [10].

At first sight, the value of the Nusselt number for the cavity at -60° (which is lower than 1) may seem doubtful because one could think that it means that the heat transfer in the cavity is smaller than what it would be in a stagnant fluid where there would be only pure conduction. Of course, this is not the case, and the value lower than 1 is entirely due to the method used to compute the average Nusselt numbers. The characteristic length (L) used in the calculation is the length of the cavity at 0° . Since the horizontal distance between the hot and the cold boundary remains the same, the effective length over which the heat transfer occurs is larger than the characteristic length for inclination angles other than 0° . Consequently, it is possible to observe a Nusselt number lower than 1. Indeed, by replacing the fluid in the cavity by a solid region having the same thermal properties as air, a Nusselt number of 0.34 is obtained, compared to the actual 0.43 for the adiabatic cavity at $\phi = -60^\circ$. The value of 0.34 therefore corresponds to the lower limit value of the Nusselt number for this configuration.

4.1.2. Combined convection-conduction enclosure

Considering the single adiabatic cavity of the previous section, two solid half-partition walls are added to the physical domain (Figure 3b). The main point of interest in this section is the combined convection-conduction heat transfer process.

To assess the importance of the conduction heat transfer in the partition walls, the thickness and the thermal conductivity ratios between the partition walls and the fluid region are var-

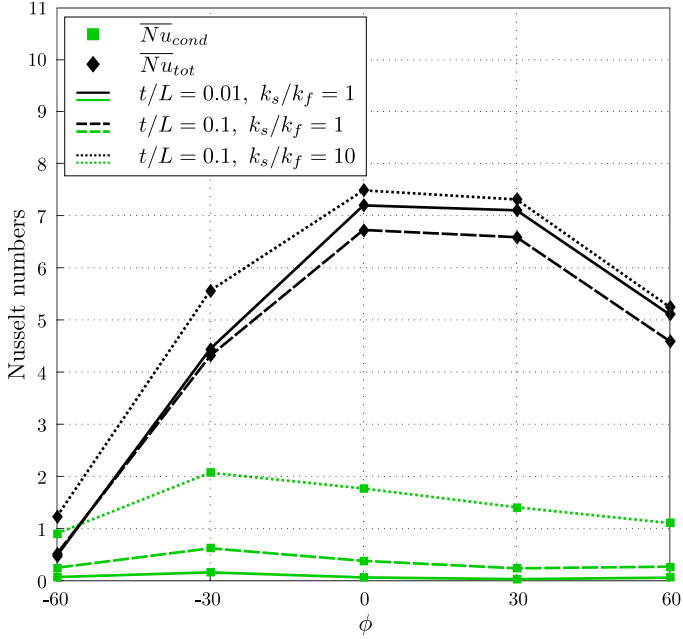


Figure 7: Conduction and total Nusselt numbers as functions of the inclination angle for three different parametric cases in a single adiabatic enclosure with solid partition walls but without radiation (physical domain of Figure 3b). Straight lines drawn between computed points are not intended for interpolation purposes.

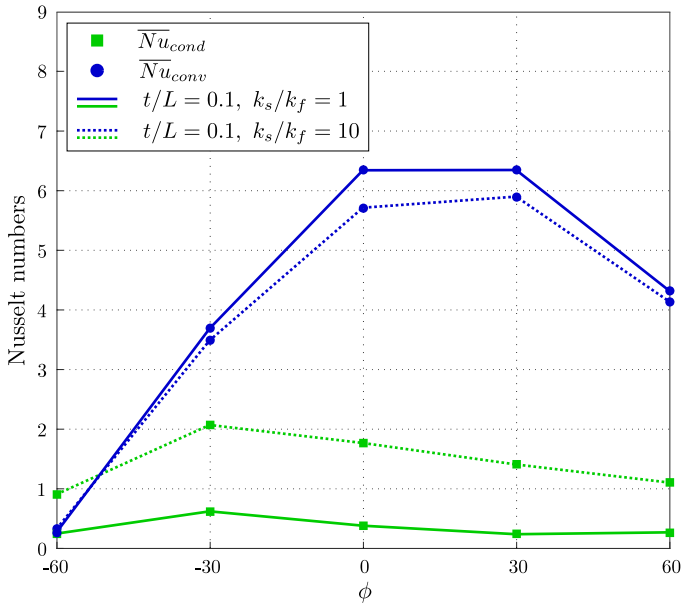


Figure 8: Conduction and convection Nusselt numbers as functions of the inclination angle for two different parametric cases in a single adiabatic enclosure with solid partition walls but without radiation (physical domain of Figure 3b). Straight lines drawn between computed points are not intended for interpolation purposes.

ied. The least conductive configuration consists of thin partition walls made of low-conductivity material ($t/L = 0.01$ and $k_s/k_f = 1$), and the most conductive case is characterized by thicker and more conductive partition walls ($t/L = 0.1$ and $k_s/k_f = 10$). Note that a thermal conductivity ratio of 10 is still low compared to the value that characterizes metallic materials like steel and aluminum (k_s/k_f would approximately be

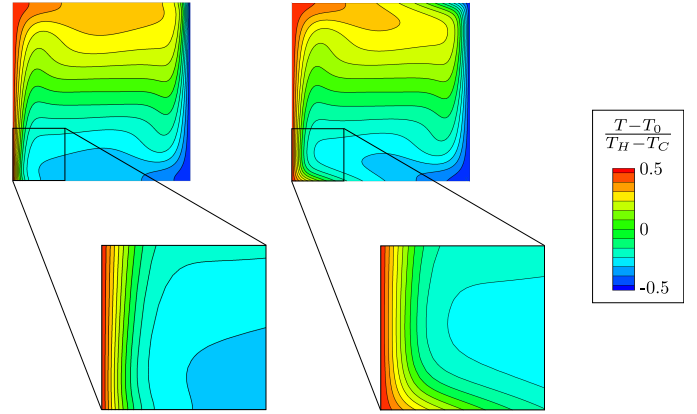


Figure 9: Temperature fields (colored background) and isotherms (black lines) in a single adiabatic cavity on the left (physical domain of Figure 3a) and in a single adiabatic enclosure with solid partition walls but without radiation on the right (physical domain of Figure 3b with $t/L = 0.1$ and $k_s/k_f = 10$; partition walls not shown).

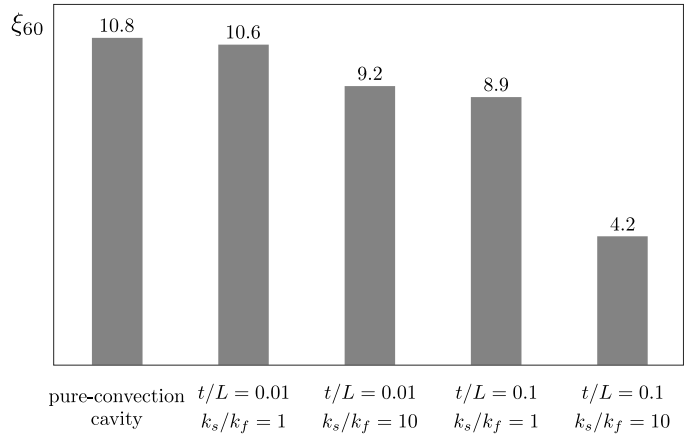


Figure 10: Thermal diode coefficient (ξ_{60}) for different parametric cases in a single adiabatic enclosure with solid partition walls but without radiation (physical domain of Figure 3b).

equal to 1 000 and 10 000 respectively).

Following this parametric study, it is found that the conduction heat transfer becomes significant for some configurations. Indeed, Figure 7 shows that the conduction may even become the dominant contribution to the total heat transfer across the enclosure for the most conductive configuration of partition walls at an inclination angle of -60° .

Moreover, the effect of conduction on the convection heat transfer in the cavity is interesting to note. As shown in Figure 8, more conductive partition walls lead to a decrease of the convection heat transfer in the cavity. The results shown in Figure 8 illustrates the importance of the interaction between the two heat transfer modes considered. The resulting decrease of convection when conduction is increased in the solid partition walls can be explained by the variation of the thermal boundary layer thickness. By varying the thermal conductivity of the solid partition walls, for a constant thickness, the temperature distribution on the upper and lower boundaries of the cavity is affected, reducing the temperature gradients of the fluid near the

vertical boundaries. In Figure 9, the temperature distributions in an adiabatic cavity without partition walls and in a cavity with the most conductive configuration of partition walls at an inclination angle of 0° are shown. Note that the partition walls have not been drawn in the figure of the enclosure located on the right in Figure 9. It can be observed that the presence of the conductive partition walls warms the fluid near the bottom left corner of the cavities. This results in the thickening of the thermal boundary layer and hence to a decrease of the temperature gradient at the boundary which in turn results in a decrease in the convection heat transfer.

Also, the thermal diode potential of the adiabatic enclosure with solid partition walls is weakened in comparison with the pure-convection cavity, as shown in Figure 10. Indeed, the thermal diode coefficient drops from $\xi_{60} = 10.8$ for the pure-convection cavity to $\xi_{60} = 4.2$ for the most conductive configuration with solid partition walls ($t/L = 0.1$ and $k_s/k_f = 10$). A part of the explanation is due to the overall increase of the total heat transfer associated to the presence of conductive solid partition walls which results in a decrease of the thermal diode potential.

4.1.3. Combined convection-radiation cavity

In this section, a domain without partition walls is considered (see Figure 3a). In order to evaluate the contribution of radiation, three different emissivity values ($\epsilon = 0$, $\epsilon = 0.1$ and $\epsilon = 0.9$) for the four inner boundaries of the cavity are considered. The value of $\epsilon = 0$ corresponds to the case treated in section 4.1.1, i.e., the pure-convection cavity.

In this study, it is systematically found that radiation contributes significantly to the total heat transfer in the cavity. As shown in Figure 11, radiation is responsible for approximately half of the global heat transfer in the cavity when the emissivity value is 0.9. Further, the impact of radiation cannot be

neglected even for the low emissivity case ($\epsilon = 0.1$).

As it has been done in the case of conduction, it is interesting to note that radiation significantly affects the convection heat transfer. Figure 12 shows the convection Nusselt numbers as a function of the inclination angle for the three different emissivity values. It is shown that for positive inclination angles, the convection heat transfer decreases when the emissivity increases and for negative inclination angles, the convection heat transfer increases with the emissivity.

In order to better understand the effect of radiation on convection, temperature fields along with stream functions are presented in Figure 13 for a positive and a negative inclination angle. The dimensionless stream function (ψ^*) shown in Figure 13 is normalized by a reference two-dimensional flowrate given by the product of the reference length and the reference velocity. For the four configurations presented in Figure 13, the increment value between each black line is constant ($\Delta\psi^* = 0.00206$), meaning that the flowrate between each streamline is the same. These stream functions clearly demonstrate the different intensities in the convective motion of the different configurations.

By definition, radiation is the electromagnetic transfer of energy that occurs without the participation of a medium between surfaces at nonzero temperatures [29]. In a closed domain like the one considered here, radiation tends to make the temperature distributions on the inner boundaries of the cavity more uniform without directly impacting the fluid itself. Since the convective motion of the fluid is caused by the difference of temperature between the boundaries, it is understandable that convection heat transfer should be affected by the radiation exchanges between these boundaries. For positive inclination angles, where the convective motion of the fluid is important, radiation tends to weaken the motion of the fluid because of its tendency to uniformize the temperature distribution. Based on the

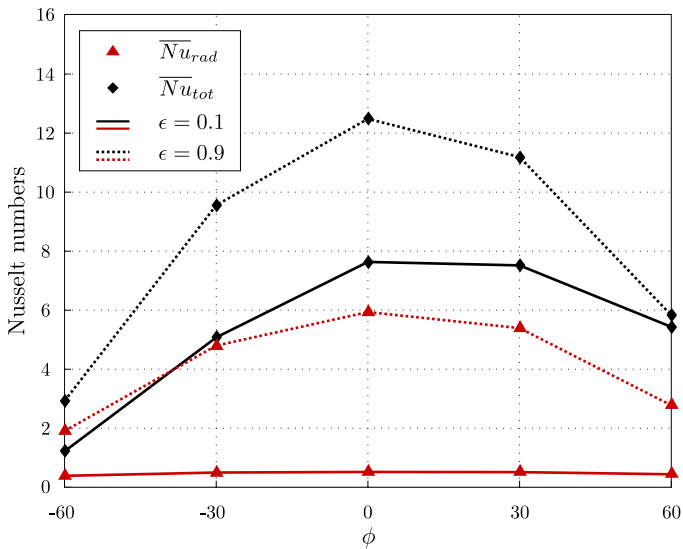


Figure 11: Radiation and total Nusselt numbers as functions of the inclination angle for two different parametric cases in a single adiabatic cavity with radiation but no partition walls (physical domain of Figure 3a). Straight lines drawn between computed points are not intended for interpolation purposes.

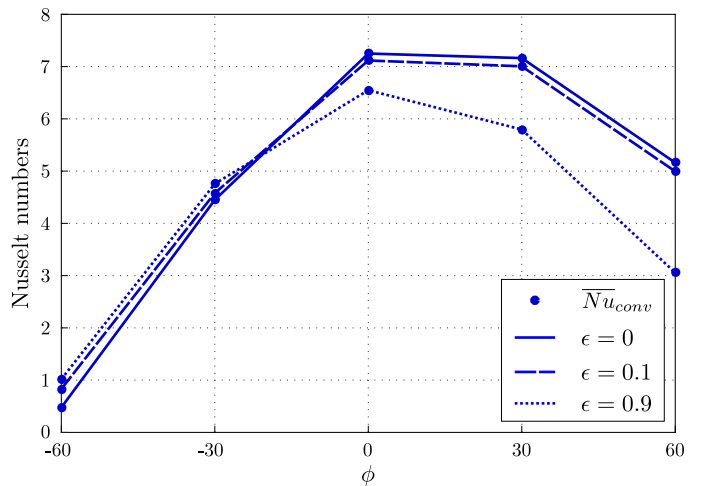


Figure 12: Convection Nusselt numbers as a function of the inclination angle for three different emissivities in a single adiabatic cavity with radiation but no partition walls (physical domain of Figure 3a). Straight lines drawn between computed points are not intended for interpolation purposes.

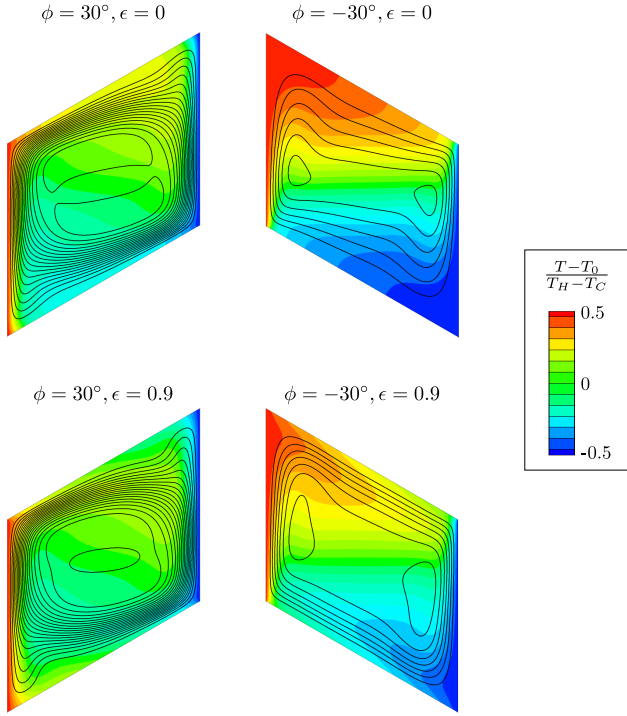


Figure 13: Temperature fields (colored background) and stream functions (black lines, $\Delta\psi^* = 0.00206$) in a single adiabatic cavity with radiation but no partition walls (physical domain of Figure 3a).

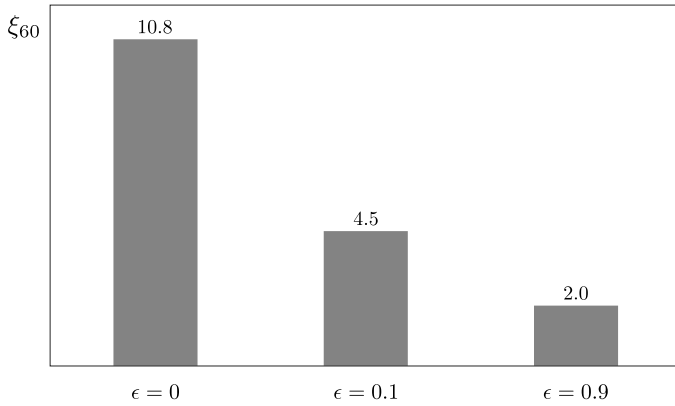


Figure 14: Thermal diode coefficient (ξ_{60}) for different parametric cases in a single adiabatic cavity with radiation but no partition walls (physical domain of Figure 3a).

same idea, for negative inclination angles, where the convective motion in the cavity is weak due to the temperature stratification in the fluid, thermal exchanges caused by radiation mitigate the temperature stratification in the fluid, and thus result in an increase of the convective motion.

The importance of radiation on the total Nusselt number is evident when comparing Figures 6 and 11. Interestingly, the red curves representing the radiation Nusselt number are mostly symmetrical around $\phi = 0^\circ$. As for conduction, it means that radiation leads to a decrease of the thermal diode potential because of the overall increase in the heat transfer for all inclination angles. Moreover, because radiation tends to attenuate the

asymmetry of the convection heat transfer, the thermal diode potential is further decreased. This is confirmed in Figure 14, which presents the thermal diode coefficient of the cavity for the three emissivity values considered. As it can be seen, the impact of radiation on the thermal diode potential is drastic. In fact, the thermal diode coefficient drops from $\xi_{60} = 10.8$ to $\xi_{60} = 4.5$, when the emissivity goes from 0 to 0.1, and drops to $\xi_{60} = 2$ when $\epsilon = 0.9$. In other words, it means that the attractive thermal diode potential of this simple adiabatic cavity is strongly reduced when radiation is taken into account.

4.1.4. Three-heat-transfer-mode enclosure

In this section, the importance and the impact of the three modes of heat transfer in a single adiabatic cavity with solid partition walls (see Figure 3b) is presented. It is found that for some parametric cases, the three modes can account more or less for the same proportion of the total Nusselt number.

As shown in Figure 15, which presents the total, the convection, the radiation and the conduction Nusselt numbers of two parametric cases as functions of the inclination angle, none of the heat transfer modes can be neglected. The two parametric cases presented in Figure 15 are, in some sense, the most extreme cases investigated. The solid-line case combines the thickest and most conductive partition walls tested along with the highest emissivity ($t/L = 0.1$, $k_s/k_f = 10$ and $\epsilon = 0.9$), while the dotted-line case corresponds to the least conductive partition walls and the lowest non-zero emissivity ($t/L = 0.01$, $k_s/k_f = 1$ and $\epsilon = 0.1$). Depending on the inclination angle and the parametric case, each heat transfer mode can become dominant. The total Nusselt numbers obtained are obviously

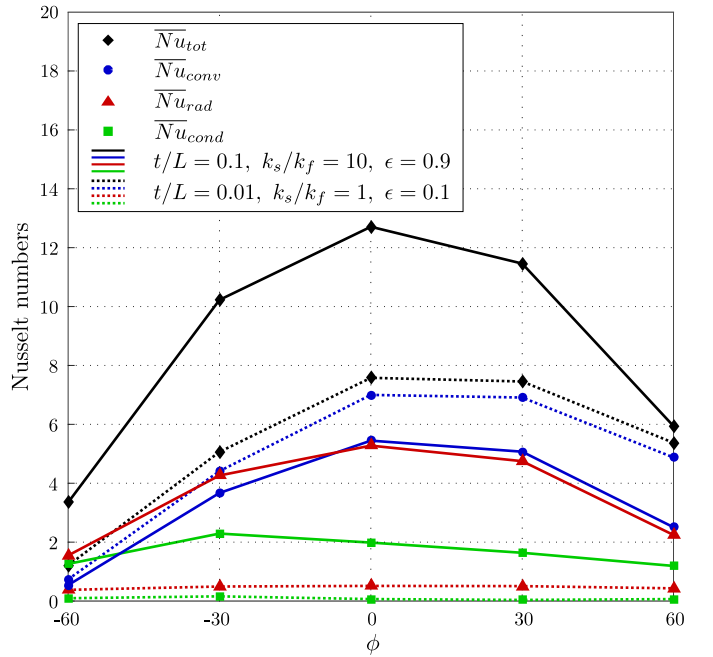


Figure 15: Total, convection, radiation and conduction Nusselt numbers as functions of the inclination angle for two different parametric cases in a single adiabatic enclosure with solid partition walls and with radiation (physical domain of Figure 3b). Straight lines drawn between computed points are not intended for interpolation purposes.

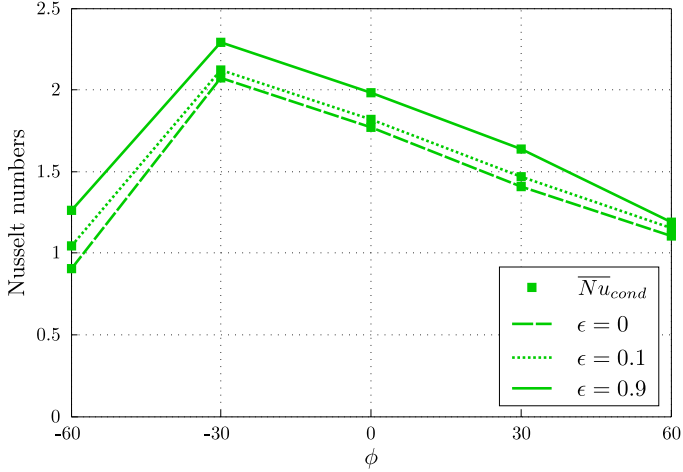


Figure 16: Conduction Nusselt numbers as a function of the inclination angle for three different emissivities in a single adiabatic enclosure with solid partition walls and with radiation (physical domain of Figure 3b). Straight lines drawn between computed points are not intended for interpolation purposes.

higher than those computed when only one or two heat transfer modes were considered. For the most conductive case investigated ($t/L = 0.1$ $k_s/k_f = 10$ and $\epsilon = 0.9$), each mode of heat transfer accounts for a significant proportion of the total Nusselt number, while the convection is clearly dominant in the least conductive configuration. In the latter, the low total Nusselt number of the enclosure at $\phi = -60^\circ$, leading to an interesting insulating character, is worth noticing.

Furthermore, it is interesting to investigate the interaction between the conduction and the radiation heat transfer in the enclosure. Actually, it is found that the emissivity of the inner boundaries of the cavity influences the conduction Nusselt number in the solid partition walls. As shown in Figure 16, which presents the conduction Nusselt number as a function of the inclination angles for different emissivity values, the conduction heat transfer increases as the emissivity increases.

Because of radiation, some of the heat from the warmer regions of the cavity's inner boundaries is transferred to the opposite colder extremities. For example, the cold extremity of the upper boundary (top right corner in Figure 3b) receives an important amount of net radiation. On the other hand, one can conceive that the left extremity of the upper boundary, which is nearly at T_H , loses an important quantity of heat through radiation. Because of the geometry and the imposed temperatures, most of the net radiation exchanges occur at the corners of the enclosure. The left part of the upper partition wall emits an important amount of energy while the upper right part receives a lot of it. This leads to an increase of the temperature gradient at the extremities of the solid partition walls and hence, to an increase in the conduction heat transfer. Based on this observation and on those made in the previous section regarding the insulating properties of an enclosure at $\phi = -60^\circ$, one can conclude that radiation is quite detrimental not only because of its own contribution to the total Nusselt number, but also because of its tendency to increase both the conduction and the convection heat transfer.

t/L	-	0.01	0.01	0.01	0.01	0.1	0.1	0.1	0.1
k_s/k_f	-	1	1	10	10	1	1	10	10
ϵ	-	0.1	0.9	0.1	0.9	0.1	0.9	0.1	0.9

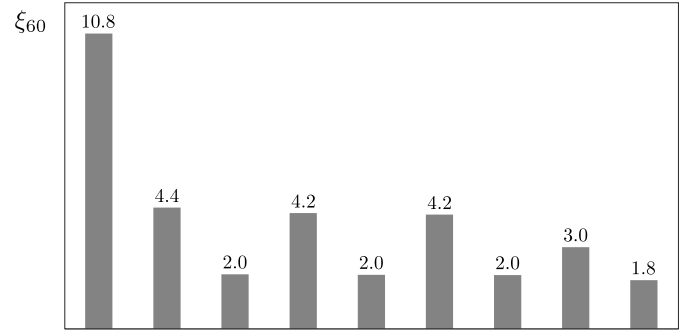


Figure 17: Thermal diode coefficient (ξ_{60}) for different parametric cases in a single adiabatic enclosure with solid partition walls and with radiation (physical domain of Figure 3b).

Lastly, Figure 17 shows the thermal diode potential for different parametric cases when the three heat transfer modes are considered. For the worst case investigated, the thermal diode coefficient falls to around $\xi_{60} = 1.8$, which is far below the promising value of $\xi_{60} = 10.8$ obtained with the pure-convection cavity.

4.2. Infinite stack of enclosures

Now that the impact of the three modes of heat transfer have been treated separately in a single adiabatic enclosure, the case of an infinite structure of piled-up enclosures is considered. The geometry used in this section is the one presented in Figure 3c.

Similarly to the three-heat-transfer-mode adiabatic enclosure discussed in the previous section, all the three modes of heat transfer account for a significant proportion of the total Nusselt number. Thus, for most of the investigated cases, they must all be taken into account to correctly capture the physics at play. Figure 18 shows the total, convection, radiation and conduction Nusselt numbers for two parametric cases of the infinite structure of piled-up enclosures. Again, the two cases presented are the two most extreme cases investigated in terms of conductive properties and emissivity.

By comparing the results of the single adiabatic enclosure (Figure 15) with those of the infinite pile (Figure 18), one can observe that the maximum values of the total Nusselt numbers are relatively similar. However, this is not true for the low- \overline{Nu}_{tot} cases. Indeed, important differences in the Nusselt numbers are noticed especially when thin partition walls are considered. The main difference observed between the single adiabatic enclosure and the infinite pile stems from the convection heat transfer. For negative inclination angles, the convection Nusselt numbers are higher in the case of the infinite pile compared to the single adiabatic enclosure while they are lower for positive inclination angles.

Figure 19, which shows the temperature fields and the stream functions of the least conductive case at $\phi = -60^\circ$, clearly demonstrates once again that the physics of the infinite structure

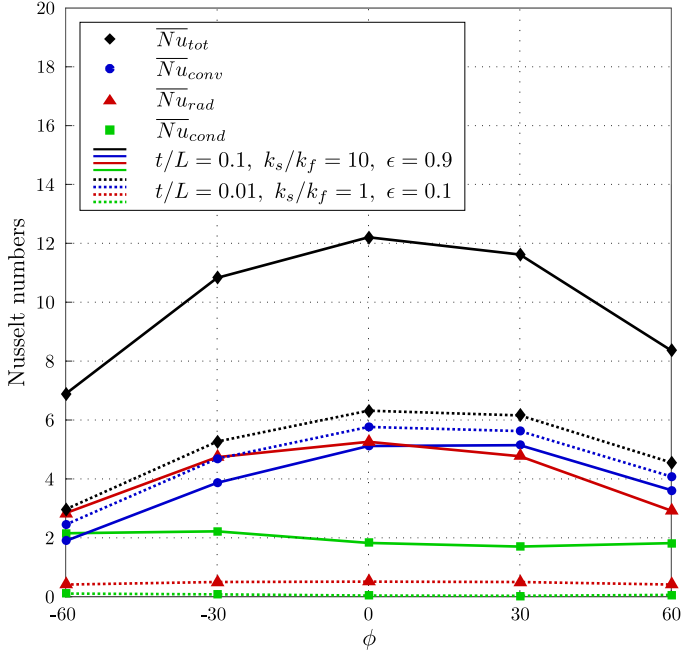


Figure 18: Total, convection, radiation and conduction Nusselt numbers as functions of the inclination angle for a infinite structure of piled-up enclosures (physical domain of Figure 3c). Straight lines drawn between computed points are not intended for interpolation purposes.

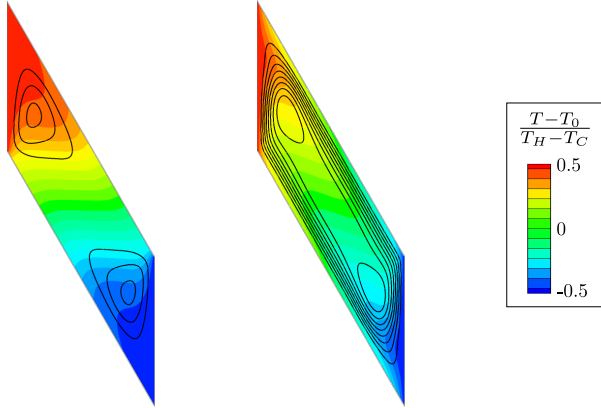


Figure 19: Temperature fields (colored background) and stream functions (black lines, $\Delta\psi^* = 0.0018$) in a single adiabatic enclosure on the left and in an infinite structure of piled-up enclosures on the right ($t/L = 0.01$, $k_s/k_f = 1$, $\epsilon = 0.1$ and $\phi = -60^\circ$).

significantly differs from the single adiabatic enclosure. As observed, the interaction between the piled-up enclosures results in a temperature distribution at the upper and lower extremities of the enclosure that is different from the distribution obtained with an adiabatic enclosure. As it can be deduced from the temperature gradients at the boundaries in Figure 19, there is a heat exchange between the piled-up enclosures with periodic boundary conditions that alters the thermal stratification which is observed in the adiabatic case. In other words, there is a net upward heat flux between the enclosures. It suggests that adiabatic enclosures may not be appropriate to model an actual piled-up structure.

t/L	-	0.01	0.01	0.01	0.01	0.1	0.1	0.1	0.1
k_s/k_f	-	1	1	10	10	1	1	10	10
ϵ	-	0.1	0.9	0.1	0.9	0.1	0.9	0.1	0.9

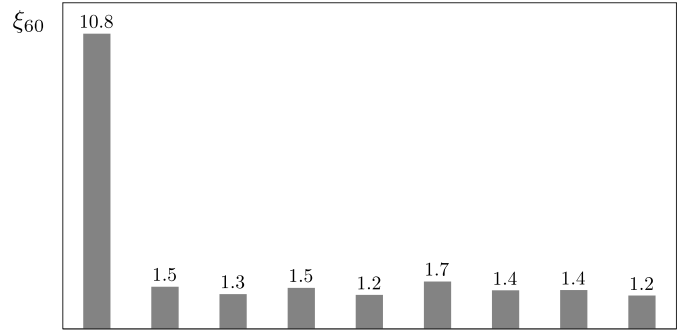


Figure 20: Thermal diode coefficient (ξ_{60}) for different parametric cases in an infinite structure of piled-up enclosures (physical domain of Figure 3c).

In the infinite pile of enclosures, the thermal diode potential is again decreased compared to the other cases presented before. Figure 20 presents the thermal diode coefficient for the same cases investigated in the previous section, but now considering the infinite structure. As it can be seen, the thermal diode coefficient drops to around $\xi_{60} = 1.4$ for most of the cases.

One notices that for applications in which the insulating properties are only required in one direction, the single adiabatic enclosure at $\phi = -60^\circ$ is approximately as good as a panel of commercial polystyrene that is widely used in insulation. However, the insulating properties are strongly affected when more than one enclosure is considered, as it can be observed in Table 3. Indeed, the total Nusselt number increases from 0.43 for a single adiabatic cavity to 2.6 when an infinite stack of enclosures involving the three heat transfer modes is considered. The difference between the total Nusselt numbers of the adiabatic enclosure and the infinite pile is significant. As mentioned previously, it mainly comes from the convection heat transfer which is much more important in the infinite structure, as it can be noticed by looking at the stream function contours in Figure 19.

The configuration of the infinite pile presented in Table 3 is the most insulating one among all the parametric cases investigated (at $\phi = -60^\circ$). In this configuration, the dominant heat transfer mode is convection. Consequently, if the objective is to further improve the insulating properties of the structure, one should seek to limit the convective fluid motion. We can expect that a pile composed of cavities having smaller aspect ratios could be efficient in that sense. Also, we have found that this can be achieved by inserting a short fin parallel to the vertical boundaries in the middle of the cavities (some sort of a fence). It would be interesting in future works to investigate if such techniques could allow lowering the total Nusselt number to a level comparable to the one of the commercial polystyrene panels while using significantly less material.

Table 3: Nusselt numbers for different cases of enclosures at $\phi = -60^\circ$ compared to a polystyrene panel.

	\overline{Nu}_{tot}	\overline{Nu}_{conv}	\overline{Nu}_{rad}	\overline{Nu}_{cond}
Infinite pile of air-filled enclosures ($t/L = 0.1$, $k_s/k_f = 1$ and $\epsilon = 0.1$)	2.60	1.67	0.34	0.59
Adiabatic enclosure ($t/L = 0.1$, $k_s/k_f = 1$ and $\epsilon = 0.1$)	1.15	0.51	0.32	0.32
Single adiabatic air-filled cavity	0.43	0.43	-	-
Commercial polystyrene panel ¹	1.09	-	-	1.09

5. Conclusion

In the present numerical study, the three modes of heat transfer through a two-dimensional stack of parallelogrammic air-filled enclosures have been investigated. For an aspect ratio of 1, a Rayleigh number of 5×10^5 , a Prandtl number of 0.71, a relative radiation level of 24.65 and a normalized mean temperature of 9.75, the importance and the interaction between each of the heat transfer modes have been discussed.

First, the importance of the conduction heat transfer in the partition walls has been demonstrated. When the partition walls are 10 times more conductive than air and 10 times thinner than the fluid cavity, conduction is the dominant heat transfer mode for highly negative inclination angles. It has also been shown that using more conductive partition walls leads to a decrease of the convective motion of the fluid.

Then, the importance of the radiation heat transfer has been exposed. For high emissivity values, radiation becomes the most important heat transfer mode in the cavities. The total Nusselt number is highly sensitive to small changes of emissivity. Moreover, it was found that the emissivity of the inner boundaries of the cavity impacts the conduction and the convection heat transfers in a significant way.

Since each heat transfer mode can be important and due to the fact that the interactions between the different modes are significant, the three of them must be taken into account in order to describe the physical phenomena occurring in the enclosures. Indeed, by neglecting one of the heat transfer mode, one does not only neglect its contribution, but also affects the other modes.

Furthermore, the thermal diode potential is strongly reduced when the complete problem is considered. In an infinite stack of enclosures, the thermal diode potential is 8 to 9 times smaller than in the single pure-convection cavity. Also, due to the convection heat transfer and to the heat exchange between the

piled-up enclosures, the insulating properties of the infinite stack are significantly reduced compared to single adiabatic enclosures, but the concept remains interesting if the insulating properties are only needed in one direction. In this context, further research needs to be devoted to the reduction of the convection heat transfer in these structures in order to obtain a better insulating structure composed of parallelogrammic air-filled enclosures. Different aspect ratios (h/L) and thicker partition walls should be primarily considered, and it would also be interesting to investigate the effects of varying the Rayleigh number.

Acknowledgments

Financial supports from the Faculté des Sciences et de Génie de l'Université Laval and the Natural Sciences and Engineering Research Council of Canada are here gratefully acknowledged.

References

- [1] A. Bejan, A synthesis of analytical results for natural convection heat transfer across rectangular enclosures, *International Journal of Heat and Mass Transfer* 23 (5) (1980) 723 – 726.
- [2] A. Bejan, *Convection Heat Transfer*, third ed., Wiley, New York, 2004.
- [3] G. De Vahl Davis, Natural convection of air in a square cavity: A benchmark numerical solution, *International Journal for Numerical Methods in Fluids* 3 (3) (1983) 249 – 264.
- [4] D.-Y. Huang, S.-S. Hsieh, Analysis of natural convection in a cylindrical enclosure, *Numerical Heat Transfer* 12 (1) (1987) 121–135.
- [5] A. H. Malik, M. Alvi, S. Khushnood, F. Mahfouz, M. Ghauri, A. Shah, Experimental study of conjugate heat transfer within a bottom heated vertical concentric cylindrical enclosure, *International Journal of Heat and Mass Transfer* 55 (4) (2012) 1154 – 1163.
- [6] J. Sieres, A. Campo, E. H. Ridouane, J. Fernández-Seara, Effect of surface radiation on buoyant convection in vertical triangular cavities with variable aperture angles, *International Journal of Heat and Mass Transfer* 50 (25-26) (2007) 5139 – 5149.
- [7] T. Basak, S. Roy, C. Thirumalesha, Finite element analysis of natural convection in a triangular enclosure: Effects of various thermal boundary conditions, *Chemical Engineering Science* 62 (9) (2007) 2623 – 2640.
- [8] V. Costa, Double-diffusive natural convection in parallelogrammic enclosures, *International Journal of Heat and Mass Transfer* 47 (14-16) (2004) 2913 – 2926.
- [9] T. Avedissian, D. Naylor, Free convective heat transfer in an enclosure with an internal louvered blind, *International Journal of Heat and Mass Transfer* 51 (12) (2008) 283 – 293.
- [10] A. Bāiri, E. Zarco-Pernia, J.-M. García de María, J.-G. Bauzin, N. Alilat, N. Laraqi, F. Gutiérrez, Nusselt-Rayleigh correlations for free convection in 2D air-filled parallelogrammic enclosures with isothermal active walls, *Heat and Mass Transfer* 47 (5) (2010) 589–595.
- [11] D. Nguyen, G. Dumas, G. Dhatt, Convection and conduction heat transfer in cavities-composed walls, in: *Proc. Fourth Int. Conf. on Num. Methods in Thermal Problems*, Vol. 1, Swansea, U.K., 1985, pp. 412–423.
- [12] H. Dixit, V. Babu, Simulation of high Rayleigh number natural convection in a square cavity using the lattice Boltzmann method, *International Journal of Heat and Mass Transfer* 49 (34) (2006) 727 – 739.
- [13] K. C. Chung, L. M. Trefethen, Natural convection in a vertical stack of inclined parallelogrammic cavities, *International Journal of Heat and Mass Transfer* 25 (2) (1982) 277 – 284.
- [14] J. M. Hyun, B. S. Choi, Transient natural convection in a parallelogram-shaped enclosure, *International Journal of Heat and Fluid Flow* 11 (2) (1990) 129 – 134.
- [15] A. Bāiri, J. García de María, I. Bāiri, N. Laraqi, E. Zarco-Pernia, N. Alilat, 2D transient natural convection in diode cavities containing an electronic equipment with discrete active bands under constant heat flux, *International Journal of Heat and Mass Transfer* 55 (19-20) (2012) 4970 – 4980.

¹<http://insulation.owenscorning.ca/assets/0/188/1c2c8d2d-4fe5-4038-970c-9028b3af7414.pdf>

- [16] R. Dalal, D. Naylor, D. Roeleveld, A CFD study of convection in a double glazed window with an enclosed pleated blind, *Energy and Buildings* 41 (11) (2009) 1256 – 1262.
- [17] A. K. Singh, S. Roy, T. Basak, Analysis of Bejan’s heatlines on visualization of heat flow and thermal mixing in tilted square cavities, *International Journal of Heat and Mass Transfer* 55 (11-12) (2012) 2965 – 2983.
- [18] G. Dumas, Simulation par éléments finis d’écoulement bi-dimensionnels avec transfert thermique, Master’s thesis, Laval University, Canada, 1985.
- [19] A. Baïri, N. Laraqi, J.-M. García de María, Numerical and experimental study of natural convection in tilted parallelepipedic cavities for large Rayleigh numbers, *Experimental Thermal and Fluid Science* 31 (4) (2007) 309 – 324.
- [20] V. Costa, M. Oliveira, A. Sousa, Laminar natural convection in a vertical stack of parallelogrammic partial enclosures with variable geometry, *International Journal of Heat and Mass Transfer* 48 (34) (2005) 779 – 792.
- [21] M. A. Antar, Thermal radiation role in conjugate heat transfer across a multiple-cavity building block, *Energy* 35 (8) (2010) 3508 – 3516.
- [22] A. Baïri, N. Laraqi, J.-M. García de María, Importance of radiative heat exchange in 2D closed diode cavities applied to solar collectors and building., *International Journal of Sustainable Energy* 24 (1) (2005) 33 – 44.
- [23] C. Balaji, S. Venkateshan, Interaction of surface radiation with free convection in a square cavity, *International Journal of Heat and Fluid Flow* 14 (3) (1993) 260 – 267.
- [24] T. Fusegi, J. Hyun, K. Kuwahara, B. Farouk, A numerical study of three-dimensional natural convection in a differentially heated cubical enclosure, *International Journal of Heat and Mass Transfer* 34 (6) (1991) 1543 – 1557.
- [25] R. Panton, *Incompressible Flow*, Wiley, New York, 1996.
- [26] ANSYS® Fluent, *Ansys fluent 14.5 user’s guide*, www.ansys.com, 2013.
- [27] J. Ferziger, M. Perić, *Computational Methods for Fluid Dynamics*, Springer, Berlin, 2002.
- [28] A. Baïri, E. Zarco-Pernia, J.-M. García de María, A review on natural convection in enclosures for engineering applications. The particular case of the parallelogrammic diode cavity, *Applied Thermal Engineering* 63 (1) (2014) 304 – 322.
- [29] T. L. Bergman, A. S. Lavine, F. P. Incropera, D. P. Dewitt, *Fundamentals of Heat and Mass Transfer*, 7th ed., Wiley, New York, 2011.